Desalination and Water Treatment
www.deswater.com

doi: 10.1080/19443994.2015.1125799

57 (2016) 21982–21989
October

Taylor & Francis
Taylor & Francis Group

Hydrothermal synthesis of NiO nanostructures for photodegradation of 4-nitrophenol

S. Safa[a], R. Hejazi[b], M. Rabbani[b], R. Azimirad[a,*]

[a]*Nanophysic group, Malek-Ashtar University of Technology, Tehran, Iran, email: Sda.safa@gmail.com (S. Safa), Tel./Fax: +98 21 22945141; email: azimirad@yahoo.com (R. Azimirad)*
[b]*Department of Chemistry, Iran University of Science and Technology, Tehran, Iran, emails: raheleh.hejazi@yahoo.com (R. Hejazi), m_rabani@iust.ac.ir (M. Rabbani)*

Received 14 April 2015; Accepted 22 November 2015

ABSTRACT

The NiO nanoparticles, nanorods, and nanoworms were synthesized by a hydrothermal reaction of $NiCl_2$ with NaC_2O_4, as a precipitation agent, and H_2O in the presence of ethylene glycol at different temperatures (100, 140, 180, and 220˚C) for 12 h. It was observed that by changing the hydrothermal temperature, one can effectively control the size and morphology of NiO nanostructures. The nanostructures were characterized by X-ray diffraction, Fourier transform infrared, scanning electron microscopy, transmission electron microscopy, and diffuse reflectance spectroscopy. Photocatalytic activity of nanostructures against 4-nitrophenol was investigated under ultraviolet and visible light irradiation. The results indicated that photocatalytic activity of NiO nanoworms synthesized at 220˚C was higher than that of the other prepared NiO nanostructures.

Keywords: Nickel oxide; Nanoworm; Photocatalyst; 4-NP

1. Introduction

Organic pollutants emitted from effluents of textile and dyeing industries are emerging as an important problem in the human food hygiene. Some of these pollutants have a considerable degree of stability in their natural cycle and they must be rapidly decomposed to become harmless species. Among them, phenol and its derivatives had been listed by Environmental Protection Agency as priority pollutants [1]. In this regard, various studies have been carried out to remove phenol-based pollutants from drinking water by chemical adsorption on porous structures [2,3] as well as catalytic [4,5] and photocatalytic degradation methods [6–8]. It is known that chemical chain reactions are generally costly and hard to use in practical conditions. Thus, photocatalytic materials like ZnO [6], TiO_2 [7], Cu_2O/TiO_2 [8] which could be activated under sunlight irradiation is preferred. On the other hand, it has been proved that the photocatalytic performance is directly dependent on active surface area of catalytic materials and therefore, nanopowders are desired. On the contrary, this procedure suffers from the widespread residue of catalytic nanopowders in processed water. In fact, the release of catalytic nanopowders into environment has raised a major concern about their potential applications [9]. The catalytic nanopowders should be either mounted on a retentive panel or easily collected from treated media.

*Corresponding author.

Recently, we proposed a method for direct growth of $CuO/Cu(OH)_2$ nanohierarchicals on Cu-foil for photocatalytic antibacterial [10] and antifungal [11] applications. Akhavan et al. [12] found an amazing photocatalytic performance of ZnO nanorods grown on glass substrate under ultraviolet (UV) irradiation. Nevertheless, in spite of considerable surface area of these nanostructures, one can use a restricted amount of these photocatalytic active panels in practical applications (only on the walls of purification pool) but for a flash treatment by an unlimited amount of nanopowder, photocatalysis is preferred. Therefore, it is necessary to find a low-cost photocatalyst which can be easily collected from purified water. Among various metal oxides, NiO has recently received increasing attention [13–17] for the reason that its photocatalytic performance is tailored to superparamagnetic properties [13]. Therefore, it can be easily recycled in water purification batches by using a magnetic field. Also, it is worthy to note that NiO nanostructure provides two other advantages in photocatalytic reactions. Firstly, it can adsorb most of the pollutant molecules due to its polar surface. The (1 1 1) surface of NiO is charged and has a dipole moment in the repeat unit perpendicular to the surface which is thought to influence adsorption processes [14]. Secondly, the oxygen atoms of NiO lattice can gradually release to surrounding environment (due to relatively low binding energy) and thereby, superoxide radicals would be formed which can greatly enhance the degradation of phenol [15]. Owing to the aforesaid advantages, many researches have been carried out for evaluating the NiO performance against UV and/or visible light activity against Rhodamine B [14], EDTA [15], etc.

Although, various works have been focused on the photocatalytic properties of NiO nanostructures, a definite understanding of the size and morphology effects of NiO on its performance is still lacking. In this paper, NiO nanostructures were synthesized and compared to each other with UV and/or visible light photoactivity against 4-nitrophenol (4-NP) pollutant. For synthesis of the various morphologies (from nanoparticles to nanorods), hydrothermal method was adopted; because, this method can be readily concerned for large scale production and offers the required flexibility [17]. Afterward, the kinetic constants of 4-NP dye removal from aqueous solutions were calculated and compared.

2. Experimental details

2.1. Materials and methods

All reagents used in this study were in analytical grade without further purification. NiO nanostructures were prepared by hydrothermal method, in which $NiCl_2{\cdot}6H_2O$, $Na_2C_2O_4$, and ethylene glycol (EG) were used as reagents. In a typical procedure [18], 0.0603 g of $Na_2C_2O_4$ was dissolved in a solution combined of 9.0 ml deionized water and 16.0 ml EG. Then, the solution was added to 1 mmol of $NiCl_6{\cdot}H_2O$ under magnetic stirring at room temperature. Afterward, the obtained clear solution was transferred into a 100 ml Teflon-lined stainless steel autoclave and kept for 12 h at different temperatures (100, 140, 180, and 220˚C). The hydrothermal products were collected and washed thrice with distilled water and absolute ethanol. Finally, the obtained products were calcinated at 400˚C for 2 h. The prepared NiO synthesized at the autoclave temperatures of 100, 140, 180, and 220˚C were denoted as NiO-100, NiO-140, NiO-180, and NiO-220, respectively.

2.2. Characterizations

Phase formation and crystalline properties of the samples were examined by an X-ray diffraction (XRD) method using an EQUINOX 3000, INEL diffractometer with a Cu k_α radiation source. The morphology of the prepared NiO nanostructures was observed by a VEGA TESCAN II scanning electron microscope (SEM). The SEM samples had been coated by a thin gold film by a desktop sputtering system (Nanostructured coating Co., Iran). The optical characteristics of the samples were examined using an MPC-2200 UV–visible diffuse reflectance spectrophotometer (DRS) in the UV and visible range (wavelengths of 200–800 nm). Fourier transform infrared (FT-IR) spectra were recorded on a Shimadzu-8400S spectrometer in the range of 400–4,000 cm^{-1} with KBr pellets. To have a better knowledge about the shape and surface area of the powders, further characterization was performed on NiO-180 by a Philips-CM120 transmission electron microscope (TEM) and Brunauer, Emmett and Teller technique (BET PHS1020). A double beam UV spectrophotometer (Shimadzu UV-1700) was used for determination of 4-NP concentration in solutions after the various steps of the degradation.

2.3. Photocatalytic measurement

In a typical process, the photo-assisted reactions were carried out in a 100 ml photoreactor, which contains 50 ml of 4-NP (10 mg l^{-1}) solution and 50 mg of photocatalyst. Before the irradiation, the solution was stirred in dark (60 min), aiming to find an equilibrium point between adsorption and desorption of 4-NP molecules on the surface of each sample. The

photocatalytic procedures were carried out under both visible (400 W tungsten light using a 400 nm cut-off filter) and UV (400 W) light sources, separately. The distance between photoreactor and light sources was adjusted to be 20 cm. For evaluating the dye decolorization during the various irradiation steps, 3 ml of each beaker was taken, separated from the photocatalyst by centrifugation and monitored by measuring its optical absorbance using a double beam UV–visible spectrophotometer (Shimadzu UV–1700) at 405 nm wavelength.

3. Results and discussion

3.1. Structural characterization of NiO samples

The XRD patterns of NiO nanostructures synthesized at various temperatures are shown in Fig. 1. It can be seen that crystallographic peaks of all prepared NiO samples are well matched with that of the bulk NiO (JCPDS card no. 04-0835) with a face-centered cubic structure. Moreover, the lack of any peak belonging to either other Ni-based compounds or impurities indicates that all the metastable middle compounds are completely converted to the cubic single phase. The lattice parameters of the NiO samples from (2 2 0) crystallographic plane grown at 100, 140, 180, and 220°C were calculated to be 0.4198, 0.4192, 0.4184, and 0.4178 nm, respectively. In this regard, it is important to note that lattice parameters calculated from high-angle diffraction peaks (in XRD) are more accurate than those taken from low-angle peaks [19]. It can be seen that with increase in the hydrothermal temperature, the calculated values are approaching to

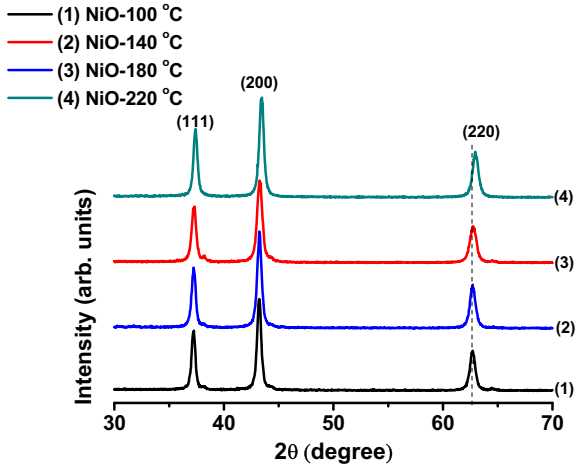

Fig. 1. XRD patterns of NiO samples synthesized at different hydrothermal temperatures of (a) 100, (b) 140, (c) 180, and (d) 220°C.

that of the bulk NiO (0.4175 nm) [19,20]. Also, the lattice crystallite size measured by the Scherrer method varies from 29 up to 36 nm for the samples grown at 100 and 220°C, respectively.

The effect of the hydrothermal temperature on the size and morphology of NiO nanostructures is depicted in Fig. 2(a)–(d). It can be seen that at low temperatures (100 and 140°C), an aggregated structure of NiO nanoparticles with an average size smaller than 50 nm is formed. Thus, it can be expected that a considerable fraction of these NiO nanostructures should be blind for the photo-assisted applications. With increasing the hydrothermal temperature to 180°C, nanorods with low aspect ratios are formed. It is seen that most of the nanorods are laterally stacked together and so, the thickness of the resulting rods are almost >100 nm (sub-micron rods). Moreover, their average aspect ratio is calculated to be ~6.5. Finally, the SEM image shown in Fig. 2(d) reveals that an inclined nanoworm-like structure of NiO with about 25 nm diameter is crystallized at 220°C. These nanoworms are irregularly spread out and as a direct result, a mostly porous structure is formed. The average aspect ratio estimated from inset of Fig. 1(d) is >40, which is significantly bigger than that of amples grown at 180°C.

Fig. 3(a) shows a typical TEM image of the sample grown at 180°C. It can be discerned from the figure that at higher magnifications, small-size nanoparticles (with average particle size ~10 nm) are well dispersed among smooth worm-like nanostructures. These nanoparticles are hardly seen at higher magnified SEM image (in the inset of Fig. 2(c)).

To validate the inner architectures of NiO nanostructure grown at 180°C, nitrogen adsorption and desorption measurements at liquid nitrogen temperature were performed. The nitrogen adsorption and desorption isotherm of the sample is shown in Fig. 3(b). The isotherm of the NiO nanostructure sample exhibits a very narrow hysteresis loop at P/P_0 range of 0.91–0.96, which shows the facile filling up and emptying of mesopore of NiO nanostructure by capillary condensation. In other words, NiO nanostructure grown at 180°C gives a facile accession to its large textural porosity. The average pore size of the NiO nanostructure was estimated to be ~2.35 nm. The BET surface area of the sample was calculated to be ~74.6 $m^2 g^{-1}$. This relatively high value can be explained by the presence of very small-size nanoparticles (as shown in TEM image) among nanoworms.

The effective surface area of the synthesized powders was qualitatively compared through monitoring the 4-NP adsorption in dark (60 min) resulting in partial decolorization of the 4-NP solutions. It was found

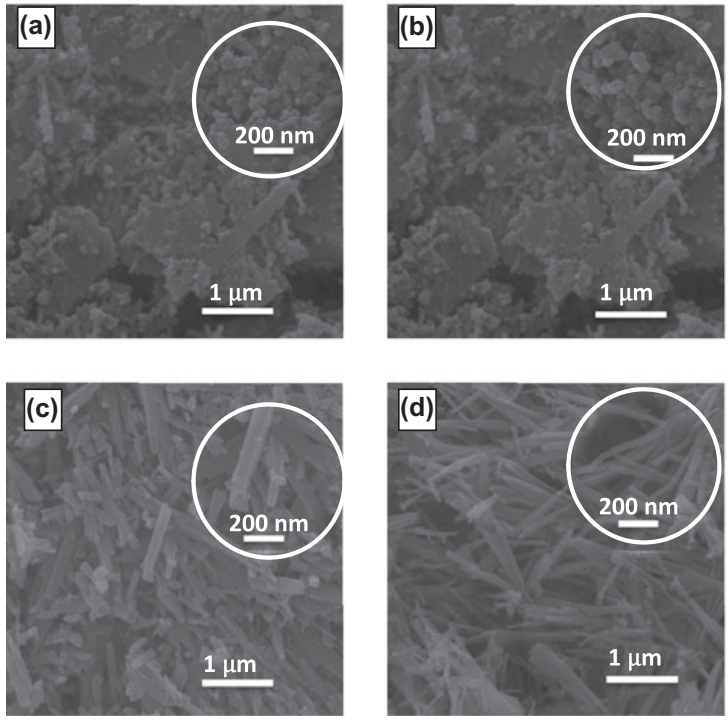

Fig. 2. SEM images of NiO nanostructures grown at hydrothermal temperatures of (a) 100, (b) 140, (c) 180, and (d) 220°C.

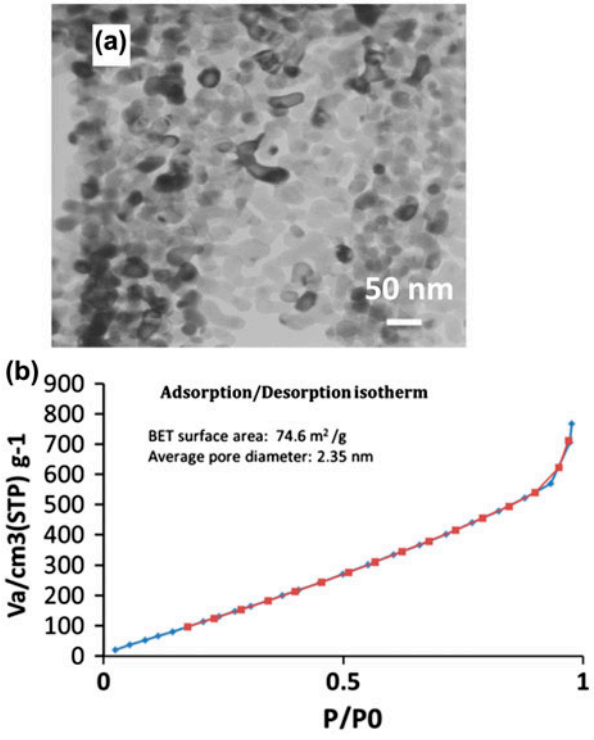

Fig. 3. (a) TEM image and (b) BET plot of the NiO nanostructure grown at 180°C.

that the solution was decolorized to ~84, 81, 80 and 77% of the control sample for NiO-100, NiO-140, NiO-180, and NiO-220, respectively. The highest surface area of NiO-220 is consistent with its morphology shown in Fig. 2.

The FT-IR spectra of NiO-220 sample before and after calcinations are shown in Fig. 4(a) and (b). For the non-calcinated sample (Fig. 4(a)), the bond at 3,450 cm^{-1} is assigned to the O–H stretching vibration. The observed bands at 2,925 and 2,847 cm^{-1} corresponded to the asymmetrical and symmetrical stretching vibrations of the $–CH_2$ surface groups, respectively. The band at 1,635 cm^{-1} is attributed to the asymmetrical stretching vibration of the C=O, and the bands at 1,317 and 831 cm^{-1} are assigned to C–O symmetrical stretching vibration and O–C=O bending vibration, respectively. The sharp band observed around 500 cm^{-1} corresponded to Ni–O stretching vibration. Besides, the FT-IR spectrum of the calcinated sample shows that almost all of the surface groups were removed by annealing at 400°C. This spectrum contains Ni–O characteristic band at 490 cm^{-1} as well as the weak and broad bands around 1,540 and 3,450 cm^{-1} assigned to the O–H stretching of absorbed water and surface O–H, respectively [21]. Therefore, the calcination process leads to formation

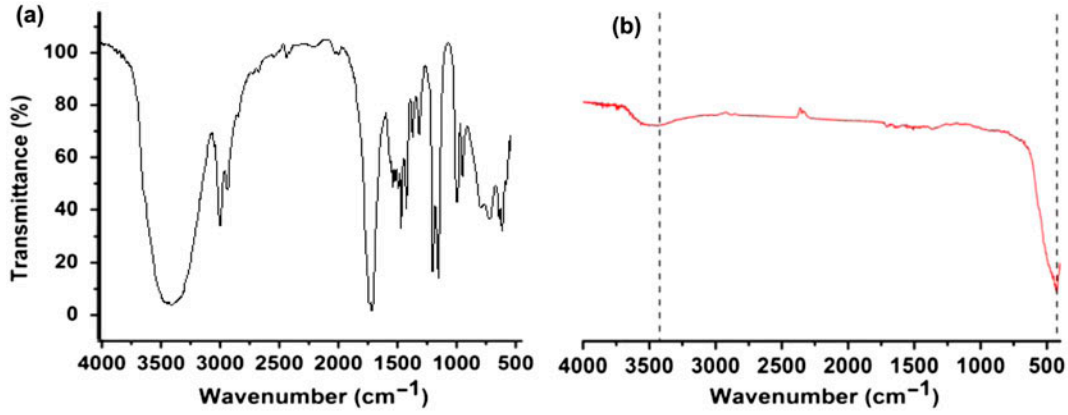

Fig. 4. FT-IR spectra of NiO-220 sample (a) before and (b) after the calcination process.

of pure NiO which is in good agreement with the XRD results.

All these results assist to predict the plausible mechanism of NiO formation. In the hydrothermal bath, thermodynamically possible chemical reactions cause the formation of $NiC_2O_4{\cdot}2H_2O$ as a metastable middle phase as follows: First $NiCl_2$ reacts with $Na_2C_2O_4$ and H_2O to form $NiC_2O_4{\cdot}2H_2O$ phase (The observed bands in FT-IR spectrum of bare sample can confirm the existence of $NiC_2O_4{\cdot}2H_2O$ phase). Afterward, the calcination of $NiC_2O_4{\cdot}2H_2O$ at 400°C would decompose it into NiO nanostructure by removing the organic groups. All of these chemical reactions are formulated as follows:

$$NiCl_2 + Na_2C_2O_4 + 2H_2O \leftrightarrow NiC_2O_4{\cdot}2H_2O + 2NaCl \quad (1)$$

$$NiC_2O_4{\cdot}2H_2O \leftrightarrow NiC_2O_4 + 2H_2O \quad (2)$$

$$2NiC_2O_4 + O_2 \leftrightarrow 2NiO + 4CO_2 \quad (3)$$

3.2. Optical properties of NiO samples

The DRS of the synthesized NiO samples are shown in Fig. 5. The spectra reveal a characteristic absorption peak of NiO at about 365 nm, which can be assigned to the electron transitions from the valence band to the conduction band. For the samples, the absorption coefficient can be expressed by Tauc's relation $(\alpha h\nu)^n = A(h\nu - E_g)$ where α is the absorption coefficient, E_g is the optical band gap, A is a constant related to the effective mass, $h\nu$ is the photo energy, and n is the power depending upon the type of optical transition between the valence and conduction bands ($n = 2$ for direct and 1/2 for indirect transitions). The magnitude of E_g is determined through plotting the graph of $(\alpha h\nu)^n$ against

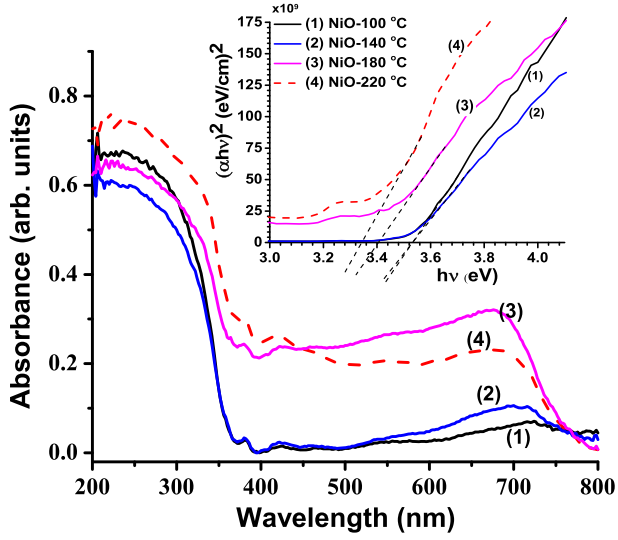

Fig. 5. DRS spectra of the NiO samples. The inset shows the plot for band gap energy (E_g) of the samples.

$h\nu$. This graph should be linear at the absorption edge. We found that the best fitting at the absorption edge can be obtained for $n = 2$, confirming the direct transition for NiO which was reported by others, too [22,23]. The value of E_g is obtained from the interception of the fitted line with the $h\nu$ axis. By this method, the value of E_g was found to be 3.52, 3.52, 3.41, and 3.34 eV for the NiO-100, NiO-140, NiO-180, and NiO-220 samples, respectively. These values are in agreement with the values reported for NiO band gap energy [23]. It is known that the chemical composition is the most important parameter on the band gap values [24]. Concerning the similarity of the chemical composition and crystal structure of the samples, the remarkable changes in the UV–visible spectra and corresponding optical

band gaps can be attributed to the morphological evolution of NiO nanostructures (from nanoparticles to nanoworms) because of the significant difference in the crystal size and pore size [25]. In fact, the mostly porous structure of nanoworms (with small pore size) allows multiple reflections of incident light and as a direct result, damping of light within the interior cavities [26]. Therefore, the decrement of optical band gap can be explained by higher polydispersity of light within the interior cavities of NiO nanoworms [27,28].

3.3. Photocatalytic performance

The photocatalytic activities of NiO catalysts were evaluated by monitoring the decolorization of 4-NP aqueous solution under UV and visible light irradiation. The characteristic absorption of 4-NP at 405 nm was chosen to monitor the photocatalytic degradation process. Fig. 6 shows a typical photocatalytic degradation process of 4-NP (initial concentration: 10 mg l^{-1}, 50 ml) using 0.05 g of NiO-220 sample under UV and visible light irradiation. The absorption peaks corresponding to 4-NP diminished gradually as the exposure time was extended. Nevertheless, one can see that 180 min of exposure is not enough for full degradation of 4-NP molecules by our photocatalyst and we just performed a comparative study in this period of time which seems to be appropriate in practical applications.

The removal efficiency of the samples was calculated from the following expression:

$$\eta = 100 \times (C_0 - C_t)/C_0 \quad (4)$$

where η is the removal efficiency; C_0 is the initial concentration of reactant; C_t is the concentration of reactant after illumination time t. Fig. 7 shows the photocatalytic removal efficiency of NiO-100, NiO-140, NiO-180, and NiO-220 as compared to the control sample (without catalyst) after 180 min irradiation.

The best photodegradation of 4-NP was carried using NiO-220 under UV light irradiation (65%) and also, under visible light irradiation (45%) which is significantly greater than the results of the other samples. The strongest UV and visible light photocatalytic activity of NiO-220 can be explained by its appropriate morphology and also, optical band gap. These parameters play an important role in the formation of high amounts of electron/hole photoexcited pairs and subsequently, high amounts of ·OH radicals to be used in degradation of 4-NP. As it is known, hydroxyl radicals are reactive species in photocatalytic process. Reaction of hydroxyl radicals with aromatic 4-NP occurs via electrophilic addition. In the presence of 4-NP, hydroxyl radicals may enter in the ortho-position to form 4-nitrocatechol (4-NC). 4-NC will react further with hydroxyl radical to form 1,2,4-benzenetriol (1,2,4-BT). Further reaction of the primary intermediates with hydroxyl radicals leads to ring opening and formation of CO_2 and H_2O products [29].

In the case of NiO nanoworms synthesized at 220°C, not only does the porous structure of sample prepare a considerable amount of direct contacts between 4-NP molecules with catalyst, but also, the lowest optical band gap of 3.34 eV for NiO-220 affords the best situation for the extended light (both UV and visible light) gain in the photocatalytic procedures. Also, it was interesting that although, all of the NiO

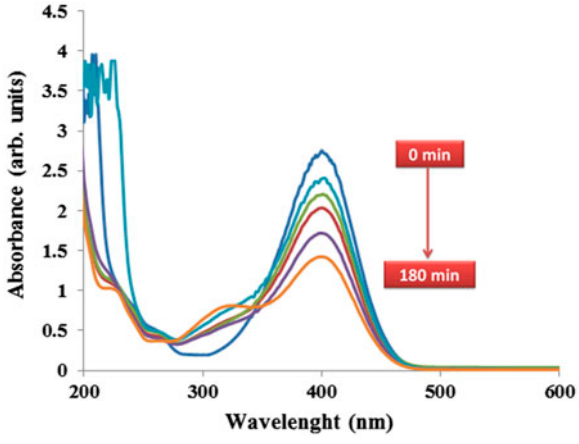

Fig. 6. The temporal evolution of the absorption spectra of the PNP solution (initial concentration: 10 mg l^{-1}, 50 ml) in presence of NiO-220 catalyst (0.05 g) under visible light irradiation.

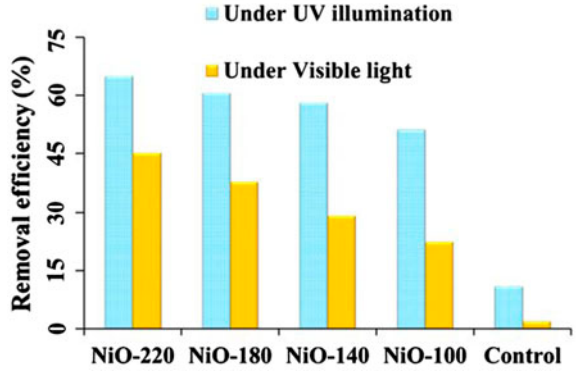

Fig. 7. The photocatalytic efficiency of NiO-100, NiO-140, NiO-180, and NiO-220 as compared to the control sample (without catalyst) after 180 min visible and UV light irradiation.

samples have the optical band gap well over 3.2 eV, 4-NP solutions are considerably degraded under visible light (with energy smaller than 3.2 eV). This phenomenon can be explained through reverse mechanism for photocatalytic removal of dye pollutants. In this mechanism, Bessekhouad et al. [30] suggested that the organic dye could be replaced by a narrow band gap semiconductor as a sensitizer. It was seen that such semiconductors in junction offer the following advantages apart from shifting the absorption. In fact, with coupling of the light-activated dye molecules and the non-activated NiO, vectorial transfer of electrons from the 4-NP to the NiO semiconductor supplies the needed electrons for the formation of ·OH radicals.

4. Conclusion

In this study, NiO nanostructures were synthesized using a simple hydrothermal method at different temperatures of 100, 140, 180, and 220˚C. It is found that the autoclave temperature effects on the size, morphology and the absorption edge of NiO nanostructures. Increasing the temperature led to the formation of nanorods with low aspect ratio and higher surface area. On the other hand, the absorption edge of NiO synthesized at the highest temperature (NiO-220) shifts to a lower energy (the entire visible region) as compared to other NiO samples. The photocatalytic degradation of 4-NP in water was studied using the prepared NiO samples under visible and UV light irradiation. Obtained results indicated that photodegradation of 4-NP was affected by the type of photocatalyst and light irradiation. In this study, NiO-220 nanoworms were found to be more efficient than NiO-100, NiO-140, and NiO-180 samples for 4-NP degradation under visible light due to their proper size and morphology as well as the lowest absorption edge.

Acknowledgment

The authors would like to thank the Iran National Science Foundation for supporting the work.

References

[1] M. Kulkarni, A. Chaudhari, Biodegradation of *p*-nitrophenol by *P. putida*, Bioresour. Technol. 97 (2006) 982–988.
[2] L. Zhu, B. Chen, Sorption behavior of p-nitrophenol on the interface BETWEEN anion−cation organobentonite and water, Environ. Sci. Technol. 34 (2000) 2997–3002.
[3] A. Walcarius, L. Mercier, Mesoporous organosilica adsorbents: Nanoengineered materials for removal of organic and inorganic pollutants, J. Mater. Chem. 20 (2010) 4478–4511.
[4] A. Zhang, N. Wang, J. Zhou, P. Jiang, G. Liu, Heterogeneous Fenton-like catalytic removal of p-nitrophenol in water using acid-activated fly ash, J. Hazard. Mater. 201–202 (2012) 68–73.
[5] J. Lee, J.C. Park, H. Song, A nanoreactor framework of a Au@SiO_2 yolk/shell structure for catalytic reduction of p-nitrophenol, Adv. Mater. 20 (2008) 1523–1528.
[6] S. Safa, R. Azimirad, R. Hejazi, M. Rabbani, ZnO hierarchical nanostructures as a powerful photocatalyst for the degradation of p-nitrophenol, Chin. J. Phys. 52 (2014) 1612–1624.
[7] G. Mele, E. Garcia-Lopez, L. Palmisano, G. Dyrda, R. Slota, Photocatalytic degradation of 4-nitrophenol in aqueous suspension by using polycrystalline TiO_2 impregnated with lanthanide double-decker phthalocyanine complexes, J. Phys. Chem. C 111 (2007) 6581–6588.
[8] L. Yang, S. Luo, Y. Li, Y. Xiao, Q. Kang, Q. Cai, High efficient photocatalytic degradation of p-nitrophenol on a unique Cu_2O/TiO_2 p–n heterojunction network catalyst, Environ. Sci. Technol. 44 (2010) 7641–7646.
[9] K.L. Dreher, Health and environmental impact of nanotechnology: Toxicological assessment of manufactured nanoparticles, Toxicol. Sci. 77 (2004) 3–5.
[10] O. Akhavan, R. Azimirad, S. Safa, E. Hasani, CuO/Cu$(OH)_2$ hierarchical nanostructures as bactericidal photocatalysts, J. Mater. Chem. 21 (2011) 9634–9640.
[11] R. Azimirad, S. Safa, Photocatalytic and antifungal activity of flower-like copper oxide nanostructures, Synth. React. Inorg., Met.-Org., Nano-Met. Chem. 44 (2014) 798–803.
[12] O. Akhavan, M. Mehrabian, K. Mirabbaszadeh, R. Azimirad, Hydrothermal synthesis of ZnO nanorod arrays for photocatalytic inactivation of bacteria, J. Phys. D: Appl. Phys. 42 (2009) 225305.
[13] Y.-J. Hao, F.-T. Li, S.-S. Wang, M.-J. Chai, R.-H. Liu, X.-J. Wang, One-step combustion synthesis of β-Bi_2O_3-NiO/Ni composites and their visible light photocatalytic performance, Mater. Sci. Eng.: B 186 (2014) 41–47.
[14] F. Motahari, M.R. Mozdianfard, M. Salavati-Niasari, Synthesis and adsorption studies of NiO nanoparticles in the presence of H_2acacen ligand, for removing Rhodamine B in wastewater treatment, Process Saf. Environ. Prot. 93 (2015) 282–292.
[15] F.A. Harraz, R.M. Mohamed, A. Shawky, I.A. Ibrahim, Composition and phase control of Ni/NiO nanoparticles for photocatalytic degradation of EDTA, J. Alloys Compd. 508 (2010) 133–140.
[16] M. Das, K.G. Bhattacharyya, Oxidation of Rhodamine B in aqueous medium in ambient conditions with raw and acid-activated MnO_2, NiO, ZnO as catalysts, J. Mol. Catal. A: Chem. 391 (2014) 121–129.
[17] X. Zhang, W. Shi, J. Zhu, W. Zhao, J. Ma, S. Mhaisalkar, T. Maria, Y. Yang, H. Zhang, H. Hng, Q. Yan, Synthesis of porous NiO nanocrystals with controllable surface area and their application as supercapacitor electrodes, Nano Res. 3 (2010) 643–652.
[18] B. Liu, H. Yang, H. Zhao, L. An, L. Zhang, R. Shi, L. Wang, L. Bao, Y. Chen, Synthesis and enhanced gas-sensing properties of ultralong NiO nanowires assembled with NiO nanocrystals, Sens. Actuators, B 156 (2011) 251–262.
[19] S.A. Speakman, Basics of X-Ray powder diffraction, Massachusetts-USA, 2010. Available from: <http://prism.mit.edu/xray>.

[20] O. Madelung, U. Rössler, M. Schulz, Non-Tetrahedrally Bonded Binary Compounds II, Springer, Verlag, Berlin, 2006.
[21] X. Liu, L. Yu, Synthesis of nanosized nickel hydroxide by solid-state reaction at room temperature, Mater. Lett. 58 (2004) 1327–1330.
[22] S. Seo, M.J. Lee, D.H. Seo, E.J. Jeoung, D.-S. Suh, Y.S. Joung, I.K. Yoo, Reproducible resistance switching in polycrystalline NiO films, Appl. Phys. Lett. 85 (2004) 5655–5657.
[23] R. Newman, R.M. Chrenko, Optical properties of nickel oxide, Phys. Rev. 114 (1959) 1507–1513.
[24] E. Kim, Z.-T. Jiang, K. No, Measurement and calculation of optical band gap of chromium aluminum oxide films, Jpn. J. Appl. Phys. 39 (2000) 4820–4825.
[25] X. Song, L. Gao, Facile synthesis and hierarchical assembly of hollow nickel oxide architectures bearing enhanced photocatalytic properties, J. Phys. Chem. C 112 (2008) 15299–15305.
[26] H. Li, Z. Bian, J. Zhu, D. Zhang, G. Li, Y. Huo, H. Li, Y. Lu, Mesoporous titania spheres with tunable chamber stucture and enhanced photocatalytic activity, J. Am. Chem. Soc. 129 (2007) 8406–8407.
[27] J. Pencer, F. Ross, Hallett, Effects of vesicle size and shape on static and dynamic light scattering measurements, Langmuir 19 (2003) 7488–7497.
[28] A.C. Holland, G. Gagne, The scattering of polarized light by polydisperse systems of irregular particles, Appl. Opt. 9 (1970) 1113–1121.
[29] N. Daneshvar, M.A. Behnajady, Y. Zorriyeh Asghar, Photooxidative degradation of 4-nitrophenol (4-NP) in UV/H_2O_2 process: Influence of operational parameters and reaction mechanism, J. Hazard. Mater. 139 (2007) 275–279.
[30] Y. Bessekhouad, D. Robert, J.V. Weber, Bi_2S_3/TiO_2 and CdS/TiO_2 heterojunctions as an available configuration for photocatalytic degradation of organic pollutant, J. Photochem. Photobiol., A 163 (2004) 569–580.